JOURNAL OF PROPULSION AND POWER
Vol. 9, No. 3, May–June 1993

Erosion Rate Diagnostics in Ion Thrusters Using Laser-Induced Fluorescence

C. J. Gaeta,* J. N. Matossian,† R. S. Turley,* J. R. Beattie,‡ J. D. Williams,§ and W. S. Williamson¶
Hughes Research Laboratories, Malibu, California 90265

We have used laser-induced fluorescence (LIF) to monitor the charge-exchange ion erosion of the molybdenum accelerator electrode in ion thrusters. This real-time, nonintrusive method was implemented by operating a 30-cm-diam ring-cusp thruster using xenon propellant. With the thruster operating at a total power of 5 kW, laser radiation at a wavelength of 390 nm (corresponding to a ground state atomic transition of molybdenum) was directed through the extracted ion beam adjacent to the downstream surface of the molybdenum accelerator electrode. Molybdenum atoms, sputtered from this surface as a result of charge-exchange ion erosion, were excited by the laser radiation. The intensity of the laser-induced fluorescence radiation, which is proportional to the sputter rate of the molybdenum atoms, was measured and correlated with variations in thruster operating conditions such as accelerator electrode voltage, accelerator electrode current, and test facility background pressure. We also demonstrated that the LIF technique has sufficient sensitivity and spatial resolution to evaluate accelerator electrode lifetime in ground-based test facilities.

Nomenclature

A_{ij} = Einstein A coefficient between levels i and j, s^{-1}
a_0 = Bohr radius, m
c = speed of light in free space, m/s
e = charge of the electron, C
f_{ij} = atomic transition oscillator strength
g = linewidth distribution function, s
$\bar{g}$ = energy averaged Gaunt factor
g_i = degeneracy for atomic level i
h = Planck's constant, J·s
$\hbar$ = Planck's constant/2π, J·s
I = intensity of optical radiation, W/m^2
J_A = accelerator electrode current, A
J_b = extracted beam ion current, A
J_E = cathode emission current, A
k = Boltzmann's constant, J/K
kT_A = temperature of molybdenum atom, eV
kT_e = electron temperature, eV
M_A = mass of molybdenum atom, kg
m_e = mass of the electron, kg
n_e = Maxwellian electron density in the extracted beam, m^{-3}
P_b = beam power, W
P_T = total thruster power, W
P_0 = vacuum chamber pressure, Pa
R_p = electron-impact excitation rate, m^3/s
R_{re} = atomic stimulated excitation rate, m^3/s
R_∞ = Rydberg energy, eV
V_A = accelerator electrode voltage, V
V_B = beam voltage, V
V_D = discharge voltage, V
Y = sputter yield, atoms/ion
ε_i = beam-ion-production cost, W/A
ε_0 = permittivity of free space, F/m
η_e = electrical efficiency, %
$(\eta_{md})_{unc}$ = discharge propellant utilization efficiency (uncorrected for doubly charged ions), %
λ = wavelength of optical radiation, m
χ_{ij} = energy difference between level i and j, eV

Received Oct. 31, 1991; revision received Nov. 2, 1992; accepted for publication Dec. 29, 1992.

*Senior Member of the Technical Staff, Optical Physics Laboratory.
†Senior Member of the Technical Staff, Plasma Physics Laboratory. Member AIAA.
‡Manager, Plasma Sources Department, Plasma Physics Laboratory. Senior Member AIAA.
§Member of the Technical Staff, Plasma Physics Laboratory. Member AIAA.
¶Project Manager, Plasma Physics Laboratory. Member AIAA.

Introduction

THE inherent low-thrust capability of ion thrusters generally dictates long operating times ranging from 4000 to 10,000 h,[1–4] depending upon thruster size and mission requirements. This, in turn, imposes a concomitant requirement on the lifetime of thruster components.

It is generally regarded that the primary lifetime-limiting wear mechanism in xenon ion thrusters is charge-exchange ion erosion of the molybdenum accelerator electrode.[5–7] This wear process has been found to be far more significant than ion erosion of the cathode and the cathode-potential screen electrode,[6] as well as the anode potential surfaces of the discharge chamber. Due to the interest in near-term applications of high power (5 kW) xenon ion thrusters, such as space vehicle orbit raising, an accurate, real-time measurement of the wear rate of the accelerator electrode is critical to providing an assessment of thruster performance and lifetime.

One method of measuring the wear rate of the accelerator electrode relies on the use of laminar thin-film badges.[8] However, this technique typically requires tests of long duration (~tens of hours) to provide an accurate assessment of component lifetime. This can restrict the quantity of test data and does not provide a real-time correlation between component wear rate, thruster operating parameters, and thruster performance.

Optical methods offer the potential of providing such a real-time data acquisition and wear rate evaluation. The use of optical emission spectroscopy[9] has been explored in order to correlate wear of the accelerator electrode in an ion thruster with measured optical emission intensity of excited sputtered molybdenum atoms. However, its use relies upon simultaneous measurements of discharge chamber plasma properties, such as electron temperature and density, as well as the solution of a system of simultaneous equations by numerical techniques to yield the wear rate. This results in an indirect assessment of the wear rate and does not occur in real-time.

We have developed and demonstrated an alternative optical diagnostic method, based on laser-induced fluorescence (LIF),[10-15] which circumvents these limitations to provide a real-time monitor of the wear rate of the molybdenum accelerator electrode in ion thrusters. This method also facilitates the correlation of accelerator electrode wear with changes in thruster performance.

The LIF technique was demonstrated by operating a 30-cm-diam ring-cusp ion thruster with xenon propellant at a nominal 5-kW power level. Charge-exchange ion erosion of the accelerator electrode resulted in a flux of molybdenum atoms downstream of the electrode. Fluorescence of the sputtered atoms was induced by an optical field from a continuous wave dye laser operating in the ultraviolet at a wavelength corresponding to a ground state transition of molybdenum. The fluorescence level, which is proportional to the density of the sputtered atoms, was correlated with variations in accelerator electrode voltage, test facility background pressure, and discharge chamber operating conditions. Although this technique has been developed specifically for ion thrusters, it is applicable to any system involving the erosion of a surface immersed in a plasma or subject to ion beam bombardment. In particular, the laser-induced fluorescence technique should provide a real-time diagnostic of cathode erosion experienced in other electric propulsion devices such as magnetoplasmadynamic (MPD) and arcjet thrusters.[16,17]

Laser-induced fluorescence is intrinsically nonintrusive and has the potential for providing high spatial resolution, real-time monitoring of the density of atomic species anywhere within a volume of interest. In addition, it can also determine the atomic state of the species.[10,11] For example, LIF has been used to determine particle densities in reactive plasmas.[15] Laser-induced fluorescence has also been used as a tool for the study of surfaces eroded by directed ion beams,[12-14] as well as surfaces immersed in a plasma.[18] In the following sections we present theoretical background and experimental results which validate the use of the laser-induced fluorescence technique as a wear rate diagnostic in ion thrusters.

Theoretical Background

In laser-induced fluorescence, atoms are stimulated by an external resonant laser source in addition to the inherent stimulation by the electrons in the plasma. The LIF signal is independent of the plasma conditions, provided the plasma does not significantly affect the density of the ground state atoms. We selected the ground state atomic transition process (λ = 390.2 nm) for molybdenum atoms that provided the largest fluorescence signal for a given laser power.

Plasmas produced in ion thruster discharge chambers are characterized as partially ionized ~10%, low pressure ~10^{-3}–10^{-2} Pa (10^{-5}–10^{-4} Torr) plasmas with an average electron temperature of 2–5 eV. Discharge chamber plasma densities are on the order of 10^{10}–10^{11}/cm^3,[19,20] while beam plasma densities are on the order of 10^9/cm^3. For the beam plasma parameters, less than 1% of the molybdenum atoms sputtered from a surface exposed to the plasma are raised to excited states as a result of collisions with electrons.[9] As a result, in order to achieve a high signal-to-noise ratio (large ratio of the laser-induced to collision-induced signals) in the laser-induced fluorescence method, the excitation of molybdenum atoms must be dominated by laser photon absorption. In order to insure this condition, we must determine the ratio of laser-induced to collision-induced excitation rates of molybdenum atoms as a function of laser intensity.

The laser-induced excitation rate can be obtained from the rate for R_{re} given in terms of the Einstein A coefficient as[21]

$$R_{re}(i \rightarrow j) = \frac{g_j}{g_i} \frac{\pi \hbar^2 c^2 I A_{ji} g}{2\chi_{ij}^3} \tag{1}$$

The Doppler distribution function g, evaluated at line center of the transition, is given by[22]

$$g = \frac{h}{\chi_{ij}} \sqrt{\frac{M_A c^2}{2\pi k T_A}} \tag{2}$$

Since the energy distribution of sputtered atoms from a surface subjected to ion bombardment is ~1–2% of the incident ion energy,[23] $kT_A \sim 1$ eV for the conditions of our experiment.

To calculate the collision-induced excitation rate for molybdenum atoms, we first note that the contributions of collisional ionization, three-body recombination, radiative recombination, dielectronic recombination, and absorption are negligible for plasmas[24] in ion thruster discharge chambers and the extracted beam. Therefore, we neglect these contributions in the theoretical development described below, and take electron-impact excitation to be the dominant reaction rate for molybdenum atoms sputtered from the accelerator electrode. More detailed quantum mechanical treatments of laser-induced fluorescence are available in the literature,[25] which account for the other effects neglected here.

The electron-impact (collision-induced) excitation rate for molybdenum atoms between states i and j, R_p $(i \rightarrow j)$, can be expressed as[26]

$$R_p(i \rightarrow j) = 16 \sqrt{\frac{2\pi}{3m_e}} \frac{R_\infty^2}{\sqrt{kT_e}\chi_{ij}} \exp\left(-\frac{\chi_{ij}}{kT_e}\right) f_{ij} \bar{g} \pi a_0^2 n_e \tag{3}$$

where the Rydberg energy R_∞ is 13.51 eV. Under our operating conditions $\bar{g}$ is assumed to be unity. The use of Eq. (3) assumes that the electron energies can be characterized by a (local) Maxwellian energy distribution which has been shown to adequately describe the electrons in the extracted ion beam.[27]

Equation (3) can be cast into a form that allows for a more convenient comparison to radiative excitation by relating the oscillator strength to the Einstein A coefficient by[21]

$$f_{ij} = \frac{4\pi\varepsilon_0 m_e c^3 \hbar^2 g_j A_{ji}}{2e^2 g_i \chi_{ij}^2} \tag{4}$$

In terms of fundamental constants and the spontaneous decay from the excited state, the plasma excitation rate is given by

$$R_p(i \rightarrow j) = 2 \sqrt{\frac{2\pi^3 m_e c^2}{3kT_e}} \frac{\hbar^2 c^2 e^2 g_j A_{ji} n_e}{4\pi\varepsilon_0 \chi_{ij}^3 g_i} \exp\left(-\frac{\chi_{ij}}{kT_e}\right) \tag{5}$$

Assuming that the decay processes and rates are the same for atoms excited by either plasma electrons or optical photons, the relative intensity of the LIF signal compared to the background (plasma-induced flourescence or PIF) signal is given by the ratio of the excitation rates for the two processes:

$$\frac{R_{re}}{R_p} = \frac{4\pi\varepsilon_0 I g}{e^2 n_e} \sqrt{\frac{3kT_e}{2\pi m_e c^2}} \exp\left(\frac{\chi_{ij}}{kT_e}\right) \tag{6}$$

The appropriate value of g to use is given by Eq. (2). Assuming kT_A = 1 eV and $2\pi\hbar c/\chi_{ij}$ = 390.2 nm yields g = 1.55×10^{-10} s. In our experiments, we used an ultraviolet beam from a Coherent 599 dye laser with an intensity of approximately 100 W/m^2 inside the vacuum test facility. Equation (6) can then be evaluated using the parameters $n_e = 6 \times 10^{15}$ m^{-3}, kT_e = 3 eV, and χ_{ij} = 3.18 eV. This gives a value of 54 for the ratio R_{re}/R_p, which is large enough to provide ample signal for determining the molybdenum density.

It is important to note that this calculation applies to the same volume of atoms for both excitation modes (plasma and radiative). In practice, the geometry of the measurement system must be considered and it is difficult to completely isolate the volume of atoms intercepted by the laser beam to avoid fluorescence contributions from other regions where the excitation mechanism is solely collisional. Although shielding was used in the experiment to minimize this additional contribution, a plasma background signal was still present. In the next section describing the experimental setup, we formulate an estimate of the geometrical effect for our measurement system which reduces the value of R_{re}/R_p from 54 to 0.3. Therefore, a phase-sensitive detection technique, described in the experimental sections, was employed and achieved a high signal-to-noise ratio. However, it was still necessary to keep the background fluorescence contribution small in order to avoid saturation of the detector.

Commercially available Ti:Sapphire lasers are much easier to maintain than a dye laser system and would probably be selected as the optical source in a practical diagnostic station. Using internal cavity doubling, these lasers can produce 200 mW of output power at 390 nm, which is resonant with the lowest lying dipole-allowed molybdenum ground state transition. If this beam is collimated to a 1-cm^2 spot, the intensity (I) would be 2000 W/m^2. This gives a value for R_{re}/R_p of 1800 for the Ti:Sapphire laser, which would correspond to an actual value of approximately 10 for the conditions of our experiment. This signal-to-noise ratio is high enough to obviate the need for phase sensitive detection methods.

We implemented the LIF technique using a dye laser system to monitor the charge-exchange ion erosion of the molybdenum accelerator electrode in a 30-cm-diam ring-cusp ion thruster. These experiments demonstrate that this technique has sufficient sensitivity and spatial resolution for evaluating accelerator grid lifetime in ground-based test facilities under typical operating conditions and in real-time. The results of these experiments, described in the following sections, validate the conclusions of the simple physical model presented above.

Experimental Setup

To demonstrate the LIF technique, a 30-cm-diam ring-cusp ion thruster was operated on xenon propellant using a two-grid extraction assembly consisting of screen and accelerator electrodes. A detailed description of the design and operating characteristics of this thruster can be found in previous publications.[7,20]

The vacuum test facility employed, illustrated in Fig. 1, is comprised of a 3-m-diam, 6-m-long chamber which is cryopumped and has a pumping speed of 135,000 l/s for xenon. The baseline pressure in the facility is 4×10^{-6} Pa (3×10^{-8} Torr).

To monitor the erosion rate of the molybdenum accelerator electrode, we note that this erosion rate is dominated by two factors: 1) the accelerator electrode voltage and 2) the charge-exchange ion density. The accelerator electrode voltage influences the erosion rate because it determines the amount of energy given to xenon charge-exchange ions that sputter the electrode. Therefore, it is important to measure the effect of accelerator voltage on the wear rate (LIF signal). Charge-exchange ions, responsible for sputtering of the accelerator electrode, are produced by the interaction of the extracted ion beam with the neutral density present in the vicinity of the accelerator electrode. For inert-gas ion thruster testing, the neutral density is typically dominated by the test facility background pressure.[7] This facility effect can result in charge-exchange-ion accelerator electrode currents far in excess of what would be experienced in an actual space environment, and is due to the finite pumping capability of ground-based test facilities. Therefore, in addition to accelerator voltage, it is important to characterize the effect of facility background pressure upon accelerator electrode wear rate. For variations of both accelerator voltage and facility background pressure, we demonstrated that the LIF technique has sufficiently high sensitivity to serve as a useful diagnostic tool for evaluating accelerator electrode wear rate in real-time for ground-based thruster testing. A discussion of the spatial resolution of the LIF technique is also presented.

Several features were incorporated in order to adapt the vacuum chamber to facilitate demonstration of the LIF technique. As shown in Fig. 1, collimators were employed to minimize the contribution of laser light scattered from surfaces within the vacuum chamber. One such collimator (6.4-cm diam) extended from the output side port into the vacuum chamber approximately 0.5 m to minimize the contribution of reflected laser light. Another was placed at the laser beam input port, located on top of the vacuum test facility, and extended approximately the same distance into the vacuum chamber. A curved quartz horn, coated with black soot from an acetylene torch, was installed at the bottom of the chamber (within another collimator) to terminate propagation of the laser light with minimum optical scattering.

Figure 2 shows a photograph of the LIF experimental setup. This arrangement employs a continuous-wave laser source consisting of a Coherent I-18 argon ion laser operating in the 350–360-nm spectral range and a Coherent 599 standing-wave tuneable dye laser capable of emitting radiation at the relevant molybdenum resonance (λ = 390 nm). The argon laser serves as an optical pump source for the dye laser. Coarse frequency tuning of the dye laser is accomplished with an intracavity birefringent plate which serves as a low loss element (Brewster angle plate) for a narrow range of frequency (~200 GHz). The absolute position of this frequency passband is adjusted by rotation of the tuning element. Etalons are also available for use within the laser cavity to spectrally narrow the laser emission to a single frequency with a jitter of less than 20 MHz. However, we determined that the birefringent tuning plate sufficiently narrowed the spectrum of the laser emission

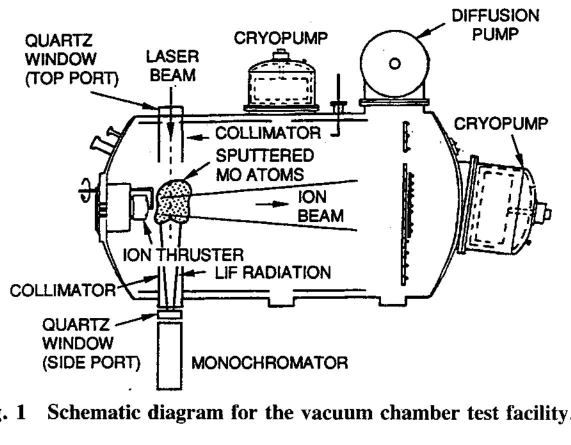

Fig. 1 Schematic diagram for the vacuum chamber test facility.

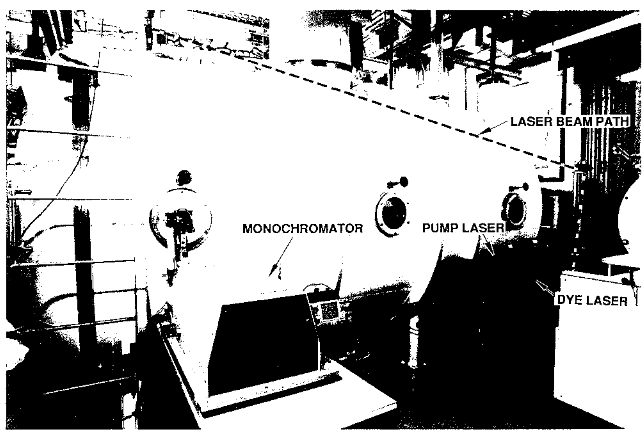

Fig. 2 Illustrated photograph showing the experimental arrangement for laser-induced fluorescence measurements.

for the purpose of our experiment (because of Doppler broadening of the atomic transition), and the etalons were not employed.

A beamsplitter directed a small portion of the output from the dye laser into a power meter in order to monitor the output power of the laser. The majority of the dye laser output was directed through the top port of the vacuum chamber using an arrangement of mirrors, as shown in Fig. 2. The laser beam then propagated through a region containing molybdenum atoms sputtered from the accelerator electrode of the ion thruster. Figure 3 (which was taken from the open end of the vacuum test chamber) shows the top port and collimator through which the laser beam enters the chamber. The collimator housing the quartz horn, which absorbs the laser radiation, is shown at the bottom of the vacuum chamber. A collimator that minimizes scattered light reaching the monochromator is visible in the right of the photograph.

A movable molybdenum plate functioned as a reflector to allow laser light, or plasma-induced fluorescence from within the discharge chamber, to reach the monochromator for calibration purposes. The molybdenum plate also served as a strong source of sputtered material which was used for initial adjustment of both the laser frequency and the monochromator wavelength.

In order to discriminate against other spectral lines, a portion of the laser-induced fluorescence was collected with a 60-cm focal length lens, directed into a Spex model 1700-11 monochromator (~0.03-nm resolution), and detected with a photomultiplier tube. The focal length of the collection lens was chosen to provide a close match to the f number of the monochromator. This procedure filled the diffraction grating in the monochromator, allowing the best spectral resolution to be realized, depending upon the width of the entrance and exit slits. These slits were wide open for our experiments (~2 mm), but this mode of operation did not adversely affect the signal-to-noise ratio.

This arrangement of the collection lens and monochromator predominantly detected light with propagation vectors parallel to the lens axis. Any other light would be shifted laterally in the focal plane (monochromator slit location) and miss the monochromator input port. Therefore, an estimate of the geometrical effect on the ratio of R_{re}/R_p may be obtained by considering a ratio of two cylindrical volumes. One volume is given by the intersection of the (1-cm diam) laser beam as it traverses molybdenum atoms within the cylindrical region defined by the collimator and the thruster beam diameter. In this volume, both LIF and PIF contributions are present in the ratio of 54:1, according to Eq. (6) and the discussion in the theoretical section. The second volume, containing molybdenum atoms excited primarily by the plasma electrons is

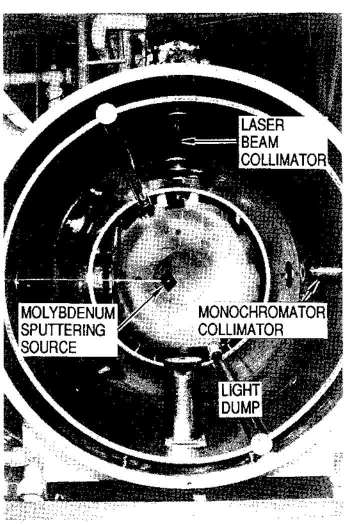

Fig. 3 Photograph of the interior of the vacuum chamber test facility.

the entire cylindrical region mentioned above. Assuming a uniform molybdenum atom density in this region, the PIF signal intercepted by the lens and directed into the monochromator is increased by the ratio of these volumes. For our experimental geometry the relevant laser beam volume is 5 cm^3, while the total volume for the PIF signal is about 900 cm^3, yielding a ratio of 5.6×10^{-3}. The ratio of R_{re}/R_p then has a corrected value of approximately 0.3 which indicates that phase-sensitive detection techniques should be adequate for the measurements.

The spatial resolution of our measurement technique, as implemented in the experiments described here, was determined by the relevant laser beam volume of 5 cm^3. Improved three-dimensional spatial resolution could be achieved by overlapping multiple laser beams in conjunction with a threshold detector. Assuming Gaussian beam propagation for the laser beams, a beam with a 1-mm-diam waist can propagate a distance of 200 cm (Rayleigh range) from the waist before the beam area doubles.[22] This suggests that fairly collimated laser beams may be overlapped to yield a resolution element of 1 mm^3. An alternative technique for accomplishing this type of resolution involves a single laser beam and a double pinhole arrangement at the detector port. One could also employ spatial filtering techniques at the light collection aperture.

We further note that the LIF technique may be extended to provide for simultaneous measurement of the erosion rates of multiple surfaces constructed with different materials. For example, to concurrently measure the erosion of the tungsten orifice plate of the hollow cathode, another laser source operating at the appropriate wavelength would be combined with the dye laser mentioned in our current experiment. A beamsplitter at the output port would then direct the output fluorescence into two separate detectors, each equipped with spectral filters, allowing selective measurement of the two fluorescence wavelengths. In a situation where all surfaces are comprised of the same material, such as molybdenum, the relative contributions to the fluorescence signal must be assessed as part of the calibration process.

LIF Experiments and Results

Prior to implementing the laser-induced fluorescence technique for measuring the charge-exchange ion erosion of the accelerator electrode in an operating ion thruster, we conducted a separate series of experiments to optimize the laser and detection system parameters.[18] In these earlier tests, we operated a discharge chamber (with the ion extraction assembly removed) and simulated the accelerator electrode with a molybdenum foil. This foil could be biased at potentials similar to those of an accelerator electrode (~100–300 V). We adapted this procedure for use in the experimental work described in this article.

The output from the dye laser was set to a wavelength corresponding to the desired molybdenum resonance (λ = 390.2 nm) using the intracavity birefringent tuning element. The laser output power during the experiment was approximately 5 mW, while the intensity within the vacuum chamber was about 100 W/m^2.

In order to further reduce the contribution from the plasma-induced fluorescence, the laser beam was amplitude modulated with a chopper at a frequency of 1 kHz. This resulted in a modulation of the LIF signal at the same frequency, in contrast to the relatively constant level of the plasma-induced background. A lock-in amplifier was then used to eliminate the dc background due to the plasma excitation. Both the dc-coupled output from the photomultiplier tube and the output from the lock-in amplifier were observed simultaneously on a dual-trace oscilloscope and a strip chart recorder.

The radiation exiting the monochromator was comprised of the LIF and PIF contributions, in addition to scattered laser light. As shown in Fig. 1, the monochromator did not have a direct line-of-sight view of the discharge chamber plasma. Although this geometry is desirable from a signal-to-noise standpoint, it makes it more difficult to set parameters such as the laser frequency and alignment of the detection system. This was accomplished using the movable molybdenum plate mentioned in the previous section. Initial alignment of the mirrors, lens and monochromator was performed by extending the plate into the flux of extracted ions so that a large plasma-induced fluorescence signal was obtained. With the plate immersed in the ion beam in this manner a copious source of sputtered molybdenum atoms was generated. When the laser beam traversed this high-density region a strong laser-induced fluorescence signal was detected, allowing for optimization of the laser wavelength and detection system parameters. Once this was accomplished, the plate was retracted and the experiments were conducted.

One of the objectives of this article is to determine the variation and sensitivity of the LIF measurement technique to changes in thruster operating parameters. Figure 4 shows the performance characteristic (variation of beam ion production cost with discharge propellant utilization efficiency) for our thruster operating at a nominal 5-kW power level. The nominal operating parameters at this power level are summarized in Table 1.

We measured the LIF signal at various points along the performance curve, and included the results in Fig. 4 for two values of the accelerator voltage. For these measurements, the beam current and discharge voltage were maintained to within ±1% of the values shown in the figure. For either value of the accelerator voltage, the LIF signal increases with decreasing propellant utilization efficiency. This behavior can

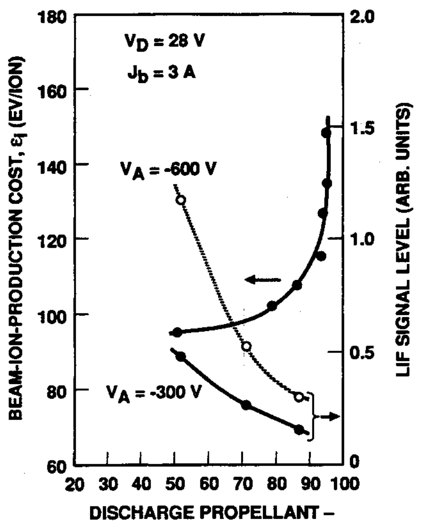

Fig. 4 Thruster performance and LIF signal as a function of discharge propellant utilization efficiency.

Table 1 Nominal thruster operating parameters

Parameter	Symbol	Units	Value
Discharge voltage	V_D	V	28
Cathode emission current	J_E	A	14
Beam-ion-production cost	ε_i	W/A	129
Extracted beam ion current	J_b	A	3
Beam voltage	V_B	V	1500
Accelerator electrode voltage	V_A	V	350
Accelerator electrode current	J_A	mA	23
Beam power	P_b	W	4560
Total thruster power	P_T	W	5024
Electrical efficiency	η_e	%	90
Discharge propellant utilization efficiency	$(\eta_{md})_{unc}$	%	86

be understood in the following manner. As the propellant utilization efficiency is reduced, the neutral loss from the thruster increases. The charge-exchange ion current, responsible for sputtering molybdenum atoms from the accelerator electrode, is proportional to the product of the beam current and the neutral loss density.[27] Therefore, the charge-exchange ion current should increase with decreasing utilization efficiency at constant beam current. This results in a corresponding increase in the sputtered molybdenum atom density, and thus the LIF signal, as shown in Fig. 4.

The data presented in Fig. 4 shows that a higher accelerator electrode voltage produces an increased LIF signal. This effect occurs because the accelerator voltage determines the energy with which the charge-exchange ions sputter the molybdenum accelerator electrode. Using the data shown in Fig. 4, we calculated the sensitivity (expressed as the fractional change in the LIF signal normalized by the coordinate of the abscissa) of the LIF signal to discharge propellant utilization efficiency. Sensitivity curves are presented in Fig. 5 for the two values of accelerator voltage. First, we note that the LIF sensitivity does not monotonically increase with decreasing utilization efficiency, in contrast to the LIF signal level, shown in Fig. 4. Second, each curve reaches a maximum sensitivity that occurs at progressively lower efficiency levels as the magnitude of the accelerator voltage is reduced. Finally, the maximum level of the sensitivity decreases with increasing accelerator voltage.

At a constant propellant utilization efficiency of 52%, we measured the variation of LIF signal with accelerator electrode voltage. The results, presented in Fig. 6, show that the LIF signal increases linearly for accelerator voltage levels up to 500 V. To gain physical insight into this behavior we included the variation of sputter yield[28] with accelerator voltage in Fig. 6 for singly charged xenon ions normally incident on a molybdenum surface. The data indicate that the LIF signal and the sputter yield have the same functional dependence on accelerator voltage up to 500 V. The LIF signal begins to saturate as the voltage is further increased. Published sputter yield data also predicts a saturation effect, but at higher voltage levels than we measured here.

The LIF data plotted in Fig. 6 were taken with a background pressure of 1.77×10^{-3} Pa (1.33×10^{-5} Torr) that resulted from the finite pumping capability of the vacuum test facility. As discussed earlier, facility background pressure affects the wear life of the accelerator electrode. Therefore, we explored the effect of facility background pressure on the LIF signal. For these measurements, the propellant utilization efficiency

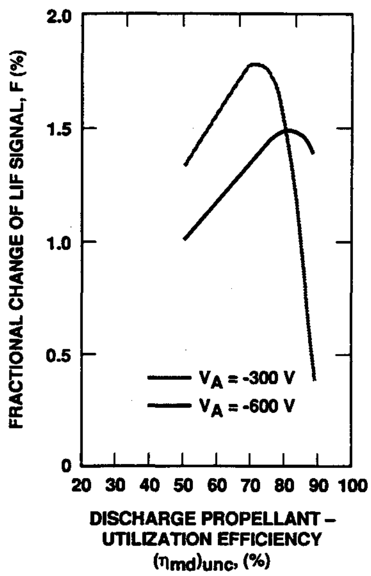

Fig. 5 Fractional change of the LIF signal level with propellant utilization efficiency.

was maintained constant while xenon gas was introduced into the vacuum chamber test facility using an auxiliary gas source. In this manner the neutral loss rate from the thruster was maintained constant so that changes in the charge-exchange-ion accelerator current were due solely to variations in facility pressure. The results of this study are presented in Fig. 7 for three different values of accelerator electrode voltage. As the accelerator voltage is increased, the LIF signal increases over the full range of pressure. This behavior is consistent with the data shown previously in Fig. 6. At the relatively low utilization efficiency (52%) used in the set of measurements shown in Fig. 7, each curve goes through a maximum value, and the pressure at which the maximum signal is obtained increases with accelerator voltage. We studied the effect of varying the utilization efficiency and the results are shown in Fig. 8. At high utilization efficiency (>70%) the LIF signal increases linearly and monotonically with pressure.

The sensitivity of the LIF signal to facility background pressure is shown in Fig. 9 for a constant propellant utilization efficiency of 52% and three values of accelerator voltage. These curves, obtained from the data in Fig. 7, show that the sensitivity is lowest where the LIF signal is highest. For constant accelerator voltage, the sensitivity increases as the pressure is lowered from the value which maximizes the LIF signal. This indicates the LIF technique is more precise at lower pressure.

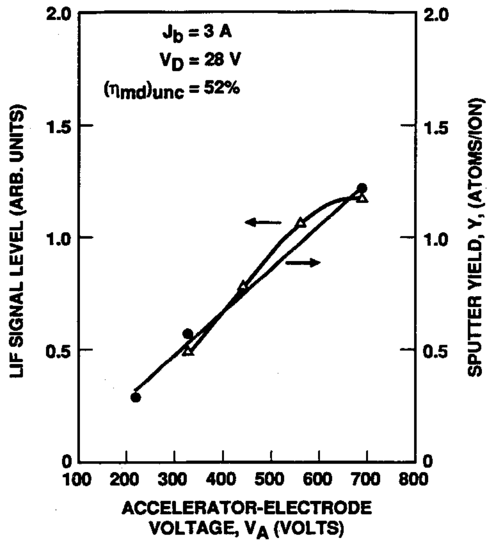

Fig. 6 Variation of the LIF signal level and sputter yield with accelerator electrode voltage (magnitude).

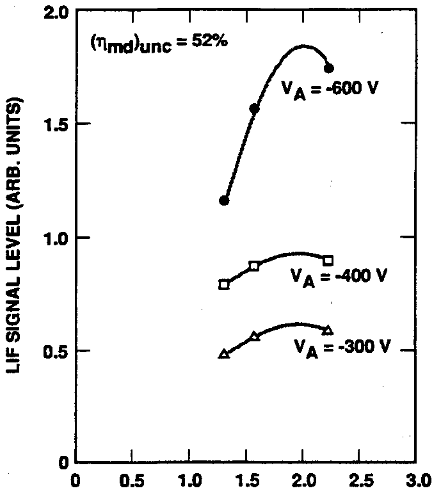

Fig. 7 Dependence of LIF signal level on externally introduced xenon gas pressure for fixed propellant utilization efficiency.

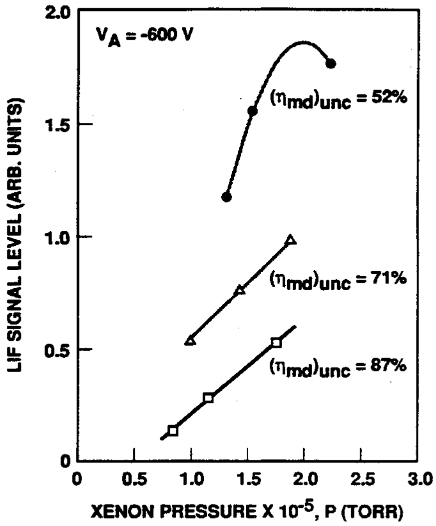

Fig. 8 Dependence of LIF signal level on externally introduced xenon gas pressure for fixed accelerator electrode voltage.

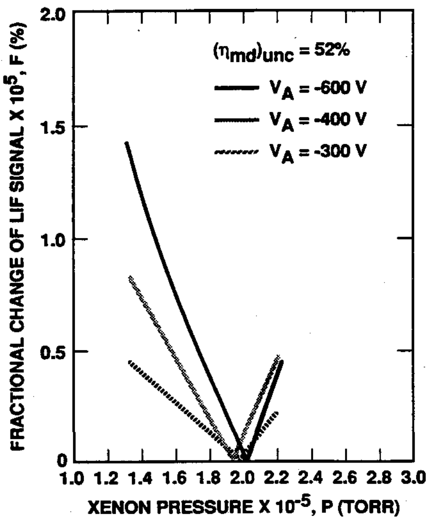

Fig. 9 Fractional change in the LIF signal with externally introduced xenon gas pressure for a fixed propellant utilization efficiency.

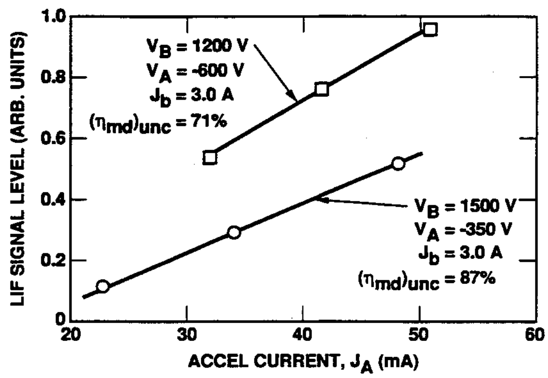

Fig. 10 Variation of the laser-induced fluorescence signal as a function of accelerator current.

In order to gain additional physical insight into the pressure dependence of the data shown in Fig. 8 we performed LIF signal measurements as a function of accelerator electrode current for two fixed values of propellant utilization efficiency, as shown in Fig. 10. The accelerator current was increased as a result of increases in pressure, obtained using the auxiliary gas source. The data shown in Fig. 10 illustrate a linear dependence of the LIF signal (molybdenum erosion rate) with accelerator electrode current for two levels of the accelerator voltage. In addition, there is an increase in the LIF signal level with accelerator electrode voltage. This behavior is consistent with the linear behavior of the LIF signal with pressure shown previously in Fig. 8, and can be understood in the following manner.[7] The total accelerator electrode current for an ion thruster is comprised of two parts[27]: 1) charge-exchange ion current and 2) direct-ion interception. Direct-ion interception is independent of the neutral gas density and depends solely upon the geometry and alignment of the ion extraction assembly apertures. The charge-exchange ion current, however, is proportional to the product of the beam current and the neutral density. For constant beam current, the charge-exchange current (and therefore, the total accelerator electrode current) increases linearly with the neutral density. By maintaining constant propellant utilization, the neutral density will only change due to variations in facility background pressure. Introducing xenon gas into the vacuum chamber under the condition of constant propellant utilization should then result in a linear increase in the density of molybdenum atoms sputtered from the electrode. The linear variation of the LIF signal with accelerator electrode current shown in Fig. 10 is consistent with this behavior. Furthermore, the relative increase in the LIF signal with accelerator voltage, also shown in the figure, is consistent with an increase in sputter yield caused by an increase in ion energy.

Conclusion

On the basis of the experimental results obtained in this study, we believe that laser-induced fluorescence can be used as a real-time diagnostic for assessing relative accelerator grid wear rates in ion thrusters. Absolute wear rates should be obtainable by calibrating the LIF signal with actual measured wear rates.

We have demonstrated the use of laser-induced fluorescence for dynamically measuring the charge-exchange ion erosion of the molybdenum accelerator electrode in xenon ion thrusters. This technique has been demonstrated at a nominal 5-kW operating power level for the thruster. The LIF signal showed excellent correlation with variations in thruster operating conditions such as accelerator electrode voltage, accelerator electrode current, and test facility background pressure. For thruster operation at high propellant utilization efficiency (>70%), the LIF signal varies linearly with the facility background pressure (or accelerator electrode current). We have also shown that the LIF technique has sufficient sensitivity and spatial resolution for use in ground-based testing of xenon ion thrusters.

The LIF method is a real-time, nonintrusive diagnostic tool which should aid in optimizing and evaluating thruster performance characteristics, as well as providing an assessment of thruster component lifetime without having to cycle through the lengthy operating times required of conventional diagnostics, such as laminar thin-film erosion badges. This technique should be widely applicable to other electric propulsion devices, such as MPD and arcjet thrusters.

Acknowledgments

This work was supported by NASA under Contract NAS 3-25553. The authors are grateful to Ross McFarlane, Jim Brown, and Robert Cronkite for the use of the lasers, as well as Coherent, Inc. for assistance on laser operation at ultraviolet wavelengths. They also thank Ray Maheux and Gunter Fehlhauer for design and fabrication of the plasma source, as well as Alan Ward for work on adapting the vacuum test facility for the LIF measurements.

References

[1]Beattie, J. R., Matossian, J. N., Poeschel, R. L., Rogers, W. P., and Martinelli, R. M., "Xenon Ion Propulsion Subsystem," *Journal of Propulsion and Power*, Vol. 5, No. 4, 1989, pp. 438–444.

[2]Beattie, J. R., and Penn, J. P., "Electric Propulsion—A National Capability," 25th Joint Propulsion Conf., AIAA Paper 89-2490, Monterey, CA, July 10–12, 1989.

[3]Schreib, R., "Electric Propulsion: Implementation Issues," 20th International Electric Propulsion Conf., AIAA Paper 88-006, Garmisch-Partenkirchen, Germany, Oct. 3–6, 1988.

[4]Birkan, M., and Micci, M. M., "Survey of Electric Propulsion Thruster Applicability to Near Earth Space Missions," 20th International Electric Propulsion Conf., AIAA Paper 88-065, Garmisch-Partenkirchen, Germany, Oct. 3–6, 1988.

[5]Beattie, J. R., and Matossian, J. N., "Xenon Ion Propulsion for Stationkeeping and Orbit Raising," 20th International Electric Propulsion Conf., Paper IEPC-88-052, Garmisch-Partenkirchen, Germany, Oct. 3–6, 1988.

[6]Beattie, J. R., Matossian, J. N., and Robson, R. R., "Status of Xenon Ion Propulsion Technology," *Journal of Propulsion and Power*, Vol. 6, No. 2, 1990, pp. 145–150.

[7]Beattie, J. R., and Matossian, J. N., "High Power Ion Thruster Technology," Hughes Research Lab., NASA CR-187161, Malibu, CA, Feb. 1992.

[8]Beattie, J. R., "A Model for Predicting the Wearout Lifetime of the LeRC/Hughes 30 cm Mercury Ion Thruster," 14th International Electric Propulsion Conf., AIAA Paper 79-2079, Princeton, NJ, Oct. 30–Nov. 1, 1979.

[9]Rock, B. A., Mantenieks, M. A., and Parsons, M. L., "Rapid Evaluation of Ion Thruster Lifetime Using Optical Emission Spectroscopy," 18th International Electric Propulsion Conf., AIAA Paper 85-2011, Alexandria, VA, Sept. 30–Oct. 3, 1985.

[10]Killinger, D. K., Wang, C. C., and Hanabusa, M., "Intensity and Pressure Dependence of Resonance Fluorescence of OH Induced by a Tunable UV Laser," *Physical Review A*, Vol. 13, No. 6, 1976, pp. 2145–2152.

[11]Heidner, R. F., III, Helvajian, H., Holloway, J. S., and Koffend, J. B., "Direct Observation of NF(X) Using Laser Induced Fluorescence: Determination of the H + NF_2 Branching Ratio," Aerospace Corp., Rept. SSD-TR-90-28, El Segundo, CA, Sept. 1990.

[12]Calaway, W. F., Young, C. E., Pellin, M. J., and Gruen, D. M., "Laser-Induced Fluorescence as a Tool for the Study of Ion Beam Sputtering," *Handbook of Ion Beam Processing Technology*, edited by J. J. Cuomo, S. M. Rossnagel, and H. R. Kaufman, Noyes Publications, Park Ridge, NJ, 1989, pp. 112–127.

[13]Bay, H. L., "Laser Induced Fluorescence as a Technique for Investigations of Sputtering Phenomena," *Nuclear Instruments and Methods in Physics Research B*, Vol. 18, 1987, pp. 430–445.

[14]Husinsky, W., "The Application of Doppler Shift Laser Fluorescence Spectroscopy for the Detection and Energy Analysis of Particles Evolving from Surfaces," *Journal of Vacuum Science and Technology*, Vol. B3, No. 5, 1985, pp. 1546–1559.

[15]Miller, T. A., "Optical Emission and Laser-Induced Fluorescence Diagnostics in Reactive Plasmas," *Journal of Vacuum Science and Technology*, Vol. A4, No. 3, 1986, pp. 1768–1772.

[16]Kurtz, H. L., Auweter-Kurtz, M., Glocker, B., Habiger, H., Merke, W., and Schrade, H. O., "Cylindrical Steady-State MPD Thruster," 20th International Electric Propulsion Conf., AIAA Paper 88-025, Garmisch-Partenkirchen, Germany, Oct. 3–6, 1988.

[17]Yoshikawa, T., Onoe, K., Yoshida, H., Kotani, S., Suzuki, H., and Uematsu, K., "Operating Characteristics of 1 kW Hydrazine Arcjet Thruster," 20th International Electric Propulsion Conf., AIAA Paper 88-108, Garmisch-Partenkirchen, Germany, Oct. 3–6, 1988.

[18]Gaeta, C. J., Turley, R. S., Matossian, J. N., Beattie, J. R., and Williamson, W. S., "Plasma Erosion Rate Diagnostics Using Laser-Induced Fluorescence," *Review of Scientific Instruments*, Vol. 63, No. 5, 1992, pp. 3090–3095.

[19]Matossian, J. N., and Beattie, J. R., "Model for Computing Volume-Averaged Plasma Properties in Electron-Bombardment Ion Thrusters," *Journal of Propulsion and Power*, Vol. 5, No. 2, 1989, pp. 188–196.

[20]Matossian, J. N., and Beattie, J. R., "Characteristics of Ring-

Cusp Discharge Chambers," *Journal of Propulsion and Power*, Vol. 7, No. 6, 1991, pp. 968–974.

[21]Stone, J. M., *Radiation and Optics*, McGraw-Hill, New York, 1963.

[22]Yariv, A., *Quantum Electronics*, 2nd ed., Wiley, New York, 1975.

[23]Kaminsky, M., *Atomic and Ionic Impact Phenomena on Metal Surfaces*, Academic Press, New York, 1965.

[24]Chapman, B., *Glow Discharge Processes*, Wiley, New York, 1980.

[25]Kimble, H. J., and Mandel, L., "Theory of Resonance Fluorescence," *Physical Review A*, Vol. 13, No. 6, 1976, pp. 2123–2143.

[26]Whitney, K. G., and Davis, J., "Hot-Spot Model of K-Line Emission from Laser-Heated Plasmas," *Journal of Applied Physics*, Vol. 45, No. 12, 1974, pp. 5294–5302.

[27]Kaufman, H. R., *Advances in Electronics and Electron Physics*, Vol. 36, Academic Press, New York, 1974, pp. 265–373.

[28]Rosenberg, D., and Wehner, G. K., "Sputtering Yields for Low Energy He^+-, Kr^+-, and Xe^+-Ion Bombardment," *Journal of Applied Physics*, Vol. 33, No. 5, 1962, pp. 1842–1845.